Live-cell super-resolution reveals F-actin and plasma membrane dynamics at the T cell synapse

George W. Ashdown, Garth L. Burn, David J. Williamson, Elvis Pandžić, Ruby Peters, Michael Holden, Helge Ewers, Lin Shao, Paul W. Wiseman and Dylan M. Owen.

ABSTRACT: The cortical actin cytoskeleton has been shown to be critical for the reorganisation and heterogeneity of plasma membrane components of many cells, including T cells. Building on previous studies at the T cell immunological synapse, we quantitatively assess the structure and dynamics of this meshwork using live-cell super-resolution fluorescence microscopy and spatio-temporal image correlation spectroscopy. We show, for the first time, that not only does the dense actin cortex flow in a retrograde fashion towards the synapse centre, but the plasma membrane itself shows similar behaviour. Furthermore, using 2-colour, live-cell super-resolution cross-correlation spectroscopy, we demonstrate that the two flows are correlated and, in addition, we show that the coupling extends to the outer leaflet of the plasma membrane by examining the flow of GPI-anchored proteins. Finally, we demonstrate that the actin flow is correlated with a third component, a-actinin, which may therefore act as an indirect linker. We hypothesise that this apparent cytoskeletal-membrane coupling could provide a mechanism for driving the observed retrograde flow of signalling molecules such as the TCR, Lck, ZAP70, LAT and SLP76.

Introduction:

Upon TCR engagement, T cells form a cell-cell junction with antigen presenting cells (APCs) termed the immunological synapse. Critical to synapse formation and stability is the cortical actin cytoskeleton[1] as well as signalling proteins residing within, and proximal to, the plasma membrane (PM). T cells actively remodel their actin cytoskeleton during synapse formation leading to cell spreading over the APC and a characteristic reorganisation of molecular

components. After remodelling, the outer zone, or dSMAC, contains a dense meshwork of actin filaments that contrasts to the centre of the synapse (cSMAC) that is actin-deficient[2]. Interestingly, in mature synapses, the actin cytoskeleton treads in a retrograde fashion from the periphery to the centre without causing cell motility[3] suggesting that actin polymerisation during and post synapse formation may have distinct and overlapping roles.

Cortical actin structure and dynamics are believed to influence signalling at the immune synapse in several ways. Firstly, proximal T cell signalling intermediates are believed to be corralled towards the central region at speeds similar to that of actin flow, where their signalling is downregulated[4,5]. Secondly, polymerised actin creates a dense meshwork which may act as a barrier for intracellular vesicle trafficking and membrane docking, spatially modulating signalling to specific regions[5,6]. In natural killer (NK) cells, the actin mesh at the cSMAC is depleted, granting cytotoxic granule passage to the membrane where they fuse and are released into the synaptic cleft to kill target cells[7–9]. Finally, it has been shown in numerous cell types that the cortical actin meshwork can influence protein diffusion within the membrane – the so-called 'picket fence model'[10] and more recently the 'active composite model'[11]. This meshwork also regulates the nanoscale clustering of certain membrane proteins[12,13].

The cortical actin meshwork and the plasma membrane may interact directly[14] or indirectly via transmembrane and scaffolding proteins[4,15,16] including TCR[17], which has been observed to cause modulation of protein lateral mobility including trapping, tethering and corralling [REFs]. These sites of interaction frequently occur at areas of high membrane lipid order[12,18,19]. Indeed, highly ordered membrane domains have been observed at the synapse periphery where cortical actin is enriched[20]. Disrupting the actin cytoskeleton disrupts membrane lipid order and de-clusters order-dependent signalling molecules such as Lck[21]. These studies suggest a relationship between actin, the plasma membrane and membrane associated proteins, however, no such actin-membrane interactions have been studied in the context of retrograde flow at the

T cell immunological synapse where the flow of actin has only been shown semi-quantitatively[3,4].

To better observe and understand these interactions, super-resolution microscopy has provided key advantages[22], including observations and mechanisms of control in nanometer scale protein cluster formation at the membrane and remodelling of actin structures[7,23,24]. Super-resolution offers a number of significant advantages over conventional fluorescence microscopy. The actin mesh density is known to be extremely high at the synapse periphery, and therefore super-resolution allows improved quantification as each pixel is not an ensemble of many individual fibres with diverse flow properties. Here, we employ single-molecule localisation microscopy (SMLM) to assess the distribution of actin at the T cell synapse with nanometre precision. In addition, we have previously demonstrated that a combination of total internal reflection (TIRF), super-resolution via structured illumination microscopy (SIM) and analysis by spatio-temporal image correlation spectroscopy (STICS[25]; Supplementary Figure 1) can quantitatively assess cortical actin flow in T cell synapses[26,27]. This is possible even in the presence of a dense meshwork and can be achieved at high spatial and temporal resolutions.

Using these methods, together with their multi-colour, cross-correlation variants, we quantitatively analyse F-actin and plasma membrane dynamics in live T cells during immunological synapse formation for the first time. After initial T cell spreading, F-actin and the peripheral regions of the plasma membrane itself flow in a retrograde manner, mirroring each other's directionality and velocity. The overall flows are both dependent on actin polymerisation, as demonstrated by the use of actin modulating drugs. Importantly, we show that both leaflets of the plasma membrane show this correlated flow with actin, as demonstrated by the observation of flow of GPI-anchored proteins in the extracellular leaflet.

There are numerous potential candidate molecules for mediating this linkage. One of these, α-actinin cross-links F-actin and plays a role in T cell synapse formation, as well as linking the cytoskeleton to transmembrane proteins and lipids[28]. α-actinin can interact simultaneously with

the cytoskeleton and distinct membrane constituents such as beta-integrin directly and indirectly through linkers such as talin and vinculin[29,30]. Via actin and protein binding domains[28,31], we hypothesised that the scaffolding function of this protein might be in part responsible for the correlation of membrane and actin flow[32]. These actin-membrane linkers may help translate F-actin's retrograde flow to the plasma membrane itself and these dynamics could hold functional importance during T cell stimulation for the translation of signalling proteins to the synapse centre, balancing prolonged signalling with signal cessation and downregulation.

Methods:

Tissue culture and sample preparation

Jurkat E6.1 T cells were cultured in RPMI + Glutamax media supplemented with 10 % FBS and 1 % PenStrep at 3-4x 10^5 / ml, and placed in a humidified 37°C environment of air + 5 % CO_2. Cells were resuspended in fresh media every 2 days and split the day prior to transfection to ensure cells were at logarithmic growth phase. For live-cell imaging Jurkat T cells were transfected with the appropriate construct(s) through electroporation (BioRad, USA). For α–actinin experiments the plasmid coded for ACTN1, transcription variant 3. Transfected cells were incubated overnight in 10mL equilibrated RPMI supplement. Primary human T cells were isolated from blood via PBMC and transfected using Amaxa (Lonza, USA) electroporation.

For PM imaging, cells were stained for 5 – 10 mins with 5 µM DiO or DiI added directly to the media before being pelleted at 268 x g for 20 s, and resuspended in an equal volume of equilibrated HBSS + 20 mM HEPES. Cells were then immediately pipetted onto the coverslip for imaging.

Integrating exchangeable single-molecule localization (IRIS) imaging is an SMLM technique which relies on capturing binding events of a probe to its target as it transiently shifts between bound and unbound states. Here a modified version of the F-actin binding peptide LifeAct, coupled to a small Atto655 molecule dye was used[33]. Fluorophore signal is captured once the

molecule is bound and localised. Cells were washed and resuspended in HBSS at 3-4x 10^5 cells / mL and dropped onto an antibody coated coverslip which was returned to the incubator for 5 mins to allow cells to form synapses. The HBSS was then removed from the wells and 200 µL of equilibrated cytoskeletal buffer (CB) + 4% PFA added to each well, coverslips were then returned to the incubator for 20mins to fix the cells. CB consisted of 10 mM MES at 6.1 pH, 5 mM MgCl, 5 mM EGTA, 150 mM NaCl and 5 mM glucose, with a final pH of 7 and stored at 4°C until the day of imaging.

After fixation cells were washed in CB and Image iT-FX Signal Enhancer (ThermoFisher) was gently added until covering the wells, this was left for 30mins at room temperature to reduce non-specific binding. Cells were then permeabilised with CB + 0.1 % Triton-X for 5 mins at room temperature, washed in CB then 0.5 nM of the LifeAct peptide conjugated to the Atto-655 probe was added providing a binding time of 20-100 ms. Conjugation was achieved through an N-terminal cysteine via maleimide chemistry.

Generating immunological synapses

To engineer T cells to produce synapses, Labtek #1.5 8-well chamber glass coverslips (Nunc, Germany) were coated with αCD3 and αCD28 antibodies (Cambridge Bioscience and BD Bioscience, UK) at a concentration of 1 µg / ml, these were left overnight at 4°C, or placed in an incubator for 2hrs. Prior to imaging, coverslips were gently washed with RT PBS to remove any antibody still in suspension and 200 µL of pre-warmed HBSS + 20mM HEPES added to each chamber.

TIRF-SIM microscope set-ups

For live-cell imaging, the microscopes incubation chamber (Tokai Hit, Japan) and heated lens collar were turned on to 37°C >2 hrs prior to imaging. For single channel TIRF-SIM on the N-SIM system (Nikon, Japan), 10 % 488 nm excitation was used, which equates to 16.5 µW in widefield mode, with a 100x 1.49 NA CFI Apochromat TIRF objective. After selecting a ROI of 512 x 512, EM Gain was set to 3 MHz at 14-bit, and EM Gain Multiplier to 300 with a Conversion Gain of 1. As the microscope relies on a physically shifting illumination pattern to achieve the 3

orientations and 3 phase shifts to create a reconstructed image, 1 frame per second was achieved when using a 50 ms frame acquisition.

Two-channel TIRF-SIM images were obtained on a Zeiss Axio Observer.Z1 (Zeiss, Germany) fitted with a spatial light modulator, producing the structured illumination pattern[34]. An Olympus 100x 1.49 NA objective (Olympus, Japan) was used, with 488 and 561 nm laser excitation and the two channel signal collected serially on two separate sCMOS cameras; to ensure minimal cross-talk a narrow band GFP filter (515/30 nm) and long pass orange/red filter (568 nm) were used. A heated chamber including humidifier (Okolab, Italy) was set to 37°C prior to imaging. Images were acquired using the same exposure time settings as the single channel datasets.

To minimise drift during single- and two-channel live cell imaging, coverslips were placed in the heated chamber for ≈ 10 minutes prior to imaging to ensure temperature equilibrium. Z-plane drift was also reduced for single-channel experiments through the perfect focus system (Nikon, Japan).

Imaging

For live-cell imaging the coated coverslip was placed in the heated incubation chamber of the microscope. 200 µL of transfected T cells were then pelleted at 268 x g for 20 s and resuspended in equilibrated HBSS + 20 mM HEPES before being carefully pipetted into one of the 8-well chambers at 3-4x 10^5 cells / mL. 5 minutes after cells landed on the coverslip TIRF-SIM acquisition of LifeAct-GFP expressing cells was carried out for 1 minute, laser illumination was set to 10 % (≈ 16.5 µW/cm^2).

For drug treatments cells were added to the coverslips and allowed to form synapses as above, then dosages were added directly to the coverslip chamber, for cytochalasin-D and jasplakinolide final concentrations were 2 µM while 7-ketocholesterol and blebbistatin were added at a final concentration of 10 and 50 µM respectively. Images were acquired as above.

IRIS imaging was carried out on the N-STORM microscope (Nikon, Japan) in TIRF mode, using a 100x 1.49 NA CFI Apochromat TIRF objective for a pixel size of 160 nm, to focus the laser intensity a collimating lens was inserted. After locating a cell using brightfield illumination, the 647 nm laser was switched on and an ROI of 512 x 512 pixels selected. Frame rates of 50 ms were used to match the binding time of the peptide[33], with the laser power set to 50 % (≈ 1.125kW/cm^2), which improved the signal to noise of bound fluorophores within the evanescent wave without increasing the background from unbound fluorophores away from the actin cortex. EM Gain was set to 17 MHz at 16-bit, and the EM Gain Multiplier to 300 with a Conversion Gain of 3. Images were acquired for 50,000 - 100,000 frames.

TIRF-SIM image reconstruction

For reconstruction of the single channel data, Nikons Analyze software (v4.20.01) was used, achieving a pixel size of 30 nm. The illumination modulation contrast (IMC) and high resolution noise suppression (HRNS) were both set to the default of 1. IMC distinguishes the stripes from the structured illumination pattern while HRNS can crop the higher resolution information from the Fourier forward transform (FFT); for the value of 1 this led to most of the higher frequency information remaining in the final image, for improved resolution.

Two-channel SIM data was reconstructed with a custom written program[35] and the reconstructed datasets were aligned using an algorithm in Priism (http://msg.ucsf.edu/IVE).

STIC(C)S settings and analysis

STICS theory has been described before[25], for our data we used the STICSGUIv0.29 (Wiseman group). For single channel F-actin datasets an analysis subregion size of 8 x 8 pixels, with a shift of 1 pixel between subregions was applied. To remove immobile and diffusive fluorescent populations prior to analysis we chose the immobile filter, set to 21 frames, removing fluorescence signal from the correlation function if it remained static for this number of frames. A polygon ROI of the cell periphery was then selected. After running the software data was saved and subregion velocity information plotted. For single-channel PM and two-channel data

a subregion size of 16 x 16 pixels and a subregion shift of 4 pixels was used, to improve the reliability of the more homogeneous signal derived from the PM.

For directionality analysis a seed point was manually chosen in the central region of the cell, each vector was then assessed against this seed point to deduce its angle of deviation, giving directional information.

IRIS analysis

Image stacks of 50,000 – 100,000 frames were analysed using the Nikon NIS analysis software (v.4.20, Nikon) with the overlapping peaks function enabled and a lower threshold of 3,000 applied. Data was reconstructed using the Nikon Imaging Software (NIS) STORM package, by scanning the image in 5x5 pixel subregions, local background is subtracted with signal above this localised by fitting an x and y Gaussian to find the centroid.

Candidate molecules are then filtered by brightness (min and max signal counts). The minimum and maximum molecule width was set to 200 nm – 400 nm, to reject noise. The localisation precision was then theoretically calculated according to the principle by[36]. The mean of the resulting localisation histogram was found to be 14 nm (n = 5). A drift correction was then applied which utilises autocorrelation to correct for gradual displacement in frames over time. Average localisation precision was extracted from the full list of emitter co-ordinates after filtering.

Statistical analysis

Analysis was carried out using a two-tailed Students t-test using GraphPad Prism version 5.00 for Windows, GraphPad Software, La Jolla California USA. Data is shown in text and plotted as means ± standard deviation.

Results:

We first imaged actin using the LifeAct probe using the IRIS approach[33], giving a mean localisation precision of 12 nm. Jurkat T cell synapses were formed using a stimulatory coverslip (Supplementary Figure 2) as previously described[27].

The data indicated a dense meshwork of actin at the synapse periphery but a relatively actin sparse region towards the centre, which contained numerous long actin fibres. Using live-cell super-resolution TIRF-SIM and cells transfected with LifeAct-GFP, we imaged the molecular flow of cortical F-actin during T cell immunological synapse formation. Using this system we were able to generate reconstructed super-resolution images of actin at a spatial resolution of ≤ 100 nm in 75 nm optical sections at 1 frame per second (Supplementary Figure 2b, Supplementary video 1). The velocity and directionality of F-actin dynamics at the observed dense, peripheral regions (Figure 1a) were quantified using STICS[25] (Figure 1b). In line with previous studies[3,4,17], actin flow had an average velocity of 1.63 ± 0.46 μm/min (Figure 1c) and was confirmed in primary human T cells 1.86 ± 0.26 μm/min (Supplementary Figure 3). Actin flow in Jurkat T cells was predominantly retrograde in nature with 72.9 % of vectors within a 90° cone directed towards the centre (Figure 1d).

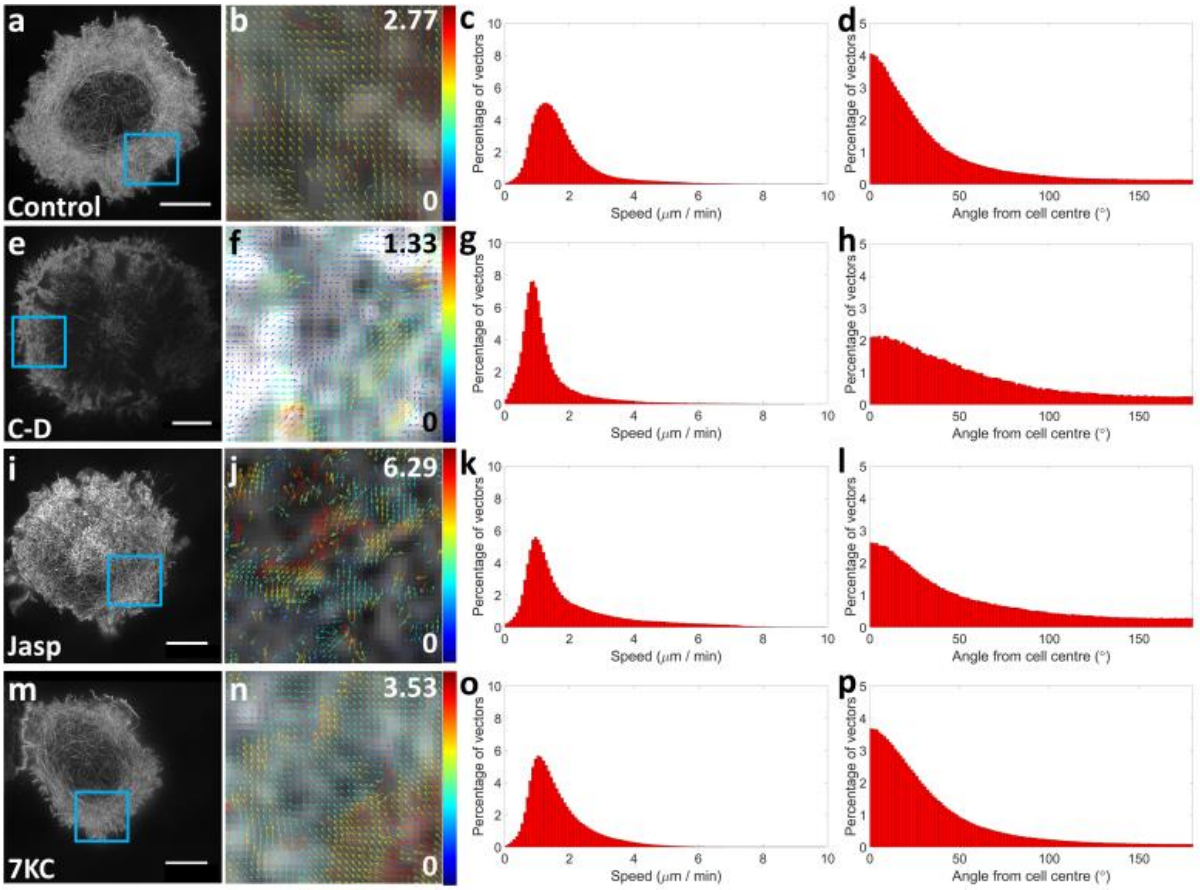

Figure 1 F-actin flow characterised using TIRF-SIM and STICS analysis. a) Images show characterisation of F-actin flow in T cells, shown are representative TIRF-SIM images (a, e, i, m) of cells 5 mins after contact with a stimulatory coverslip and following different treatments (labelled bottom left of images). ROI's within the blue boxes are to the right (b, f, j, n), showing the output vector maps from STICS analysis. Scale bar = 5 µm. b) Graphs show STICS outputs of normalised F-actin flow, any changes after drug treatment in either subregion velocity (c, g, k, o) or directionality (d, h, l, p) are plotted. (Controls: 1.63 ± 0.46 µm, n = 24. Cytochalasin-D (C-D): 0.99 ± 0.27 µm, n= 10. Jasplakinolide (Jasp): 2.07 ± 1.06 µm, n = 27. 7-Ketocholesterol (7KC): 1.61 ± 0.49 µm, n= 24.)

To ensure the high resolution noise associated with SIM images was not contributing to STICS output vectors, spatial filters were applied to actin images during the reconstruction process, degrading the resolution to conventional microscopy standards of ~ 250nm and removing these artefacts. Flow speeds and directionality are not significantly different between these conditions (Supplementary Figure 4), although some directional information was lost when correlating the lower resolution datasets.

Next, drug treatments that affect polymerization rates were used and were shown to disrupt both F-actin flow velocities and directionality. Cytochalasin-D, (Figure 1e and f) which reduces

the rate of polymerization by capping the growing end of F-actin, was found to reduce the velocity of retrograde flow to 0.99 ± 0.27 μm/min ($p < 0.001$) (Figure 1g) while also scrambling the directionality (Figure 1h) ($p = 0.01$). Jasplakinolide, which increases polymerization and stabilises actin filaments (Figure 1i and j) had no significant effect on velocity (Figure 1k) ($p = 0.06$) but did perturb directionality (Figure 1l) ($p < 0.01$). As jasplakinolide increases actin polymerisation universally, but in an uncontrolled manner, the scrambling of the directionality demonstrates the system relies on balancing polymerization and depolymerisation in a regulated fashion to achieve the ordered retrograde flow during synapse formation. To investigate whether membrane lipid order had an effect on F-actin retrograde flow, we reduced lipid order using the cholesterol analogue 7-ketocholesterol (7KC) previously demonstrated in T cells[37] (Figure 1m and n). F-actin flow velocities (Figure 1o) and directionality (Figure 1p) were not significantly altered ($p = 0.88$ and 0.32). Finally, we treated cells using Blebbistatin which inhibits Myosin II motors. In this case, no difference in flow velocities was observed between the treated cells and control cells (Supplementary Figure 3). The fact that inhibiting Myosin II motors did not slow actin retrograde flow velocity strongly suggests the actin flow is driven by actin polymerisation.

To clarify the changes all drug treatments had on actin retrograde flow we plotted the percentage change compared to control conditions (Figure 2). Positive (negative) y-axis values indicate the cells undergoing drug treatment have a greater (fewer) number of vectors at that range of velocities or angles. As expected, cytochalasin-D reduced F-actin velocity (Figure 2a and d), while jasplakinolide had no significant effect (Figure 2b and d). 7KC showed no significant differences indicating actin flow is not dependent on membrane lipid order (Figure 2c and d). These treatment conditions were shown not to adversely affect cell viability (Supplementary Figure 4).

LifeAct labels F-actin by transiently binding to multiple monomers, potentially stabilising the labelled structure. As such, we repeated the experiments of Figure 2 with monomeric GFP-actin

to label actin structures without this transient binding event (Supplementary Figure 6). The results were similar to the LifeAct results for both control and drug treatments, with CD significantly slowing actin flow ($p < 0.003$) and disrupting actin directionality ($p = 0.0005$), while jasplakinolide treated cells were not significantly different for either flow speed (0.07) or direction ($p = 0.1$) versus controls.

Studies have shown that the cortical actin meshwork and the plasma membrane may interact directly[14] or indirectly via transmembrane and scaffolding proteins[4,15,16]. We therefore hypothesised that the flow of the cortical actin mesh might be coupled to the membrane, causing retrograde membrane flow. Cells were stained with the lipophilic membrane dye DiO, synapses were formed on activating coverslips with cells imaged by TIRF-SIM (Supplementary video 2) and membrane flow quantified by STICS. Our data indicated that the membrane also flows in a retrograde fashion (63.3 % inward) with a velocity comparable to that of actin (Figure 4a and b). In the actin-poor synapse centre, vector directionality exhibited near homogenous distribution across all angles (Supplementary Figure 7).

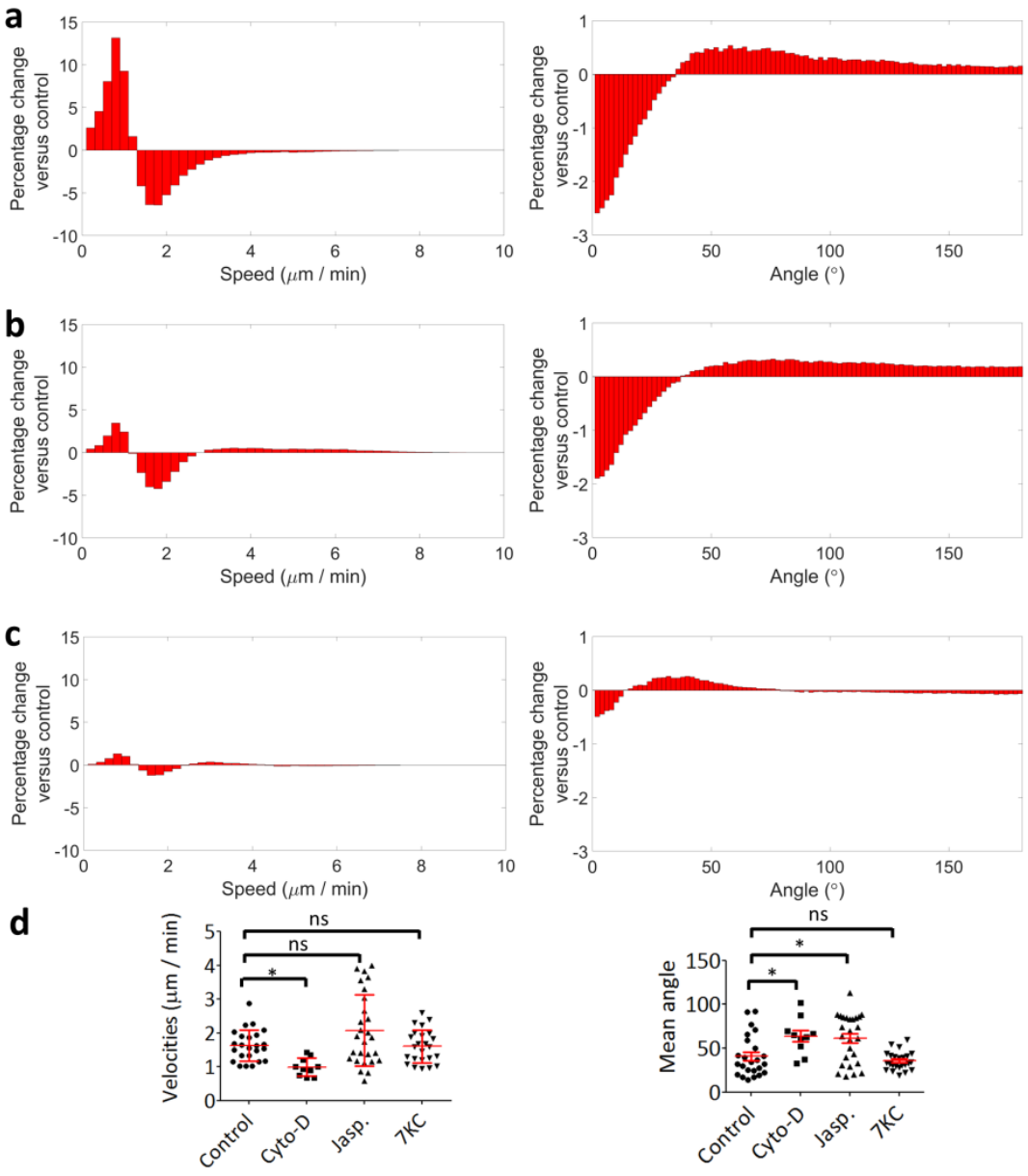

Figure 2 Characterisation of F-actin flow in drug treated T cells compared with control conditions. Vector distribution differences of cellular F-actin after drug treatments when compared with control cells. Positive (negative) x-axis values represent bins where the drug treatment cells exhibit greater (lower) numbers of vectors. Cytochalasin-D treated cells (a) have a significant shift towards slower moving vectors (exhibiting a positive or leptokurtic distribution) and have less retrograde directionality when compared with control cells. Jasplakinolide treated cells (b) exhibit a spread distribution (platykurtic) of vector speeds compared with control cells, with vectors populating slower and faster velocities, there is also a similar disruption of directionality. Through disruption of membrane lipid order with the addition of methyl-β cyclodextrin and 7-ketocholesterol (c) a less dramatic but similar platykurtic distribution was observed for vector speeds and directionality was also disrupted but to a lesser extent than actin modulating drugs. d) Scatterplots of mean cell velocities (left) and angles (right) for different drug treatments. Compared to control cells, cytochalasin-D treated cells had significantly slower ($p < 0.001$) average speeds. For directionality, the actin-modulating cytochalain-D increased the mean angle significantly ($p = 0.01$), as did jasplakinolide ($p = 0.008$) indicating polymerization drives retrograde flow order. The disruption of membrane order had no significant effect on the speed or directionality of cell means ($p = 0.88$ and 0.32).

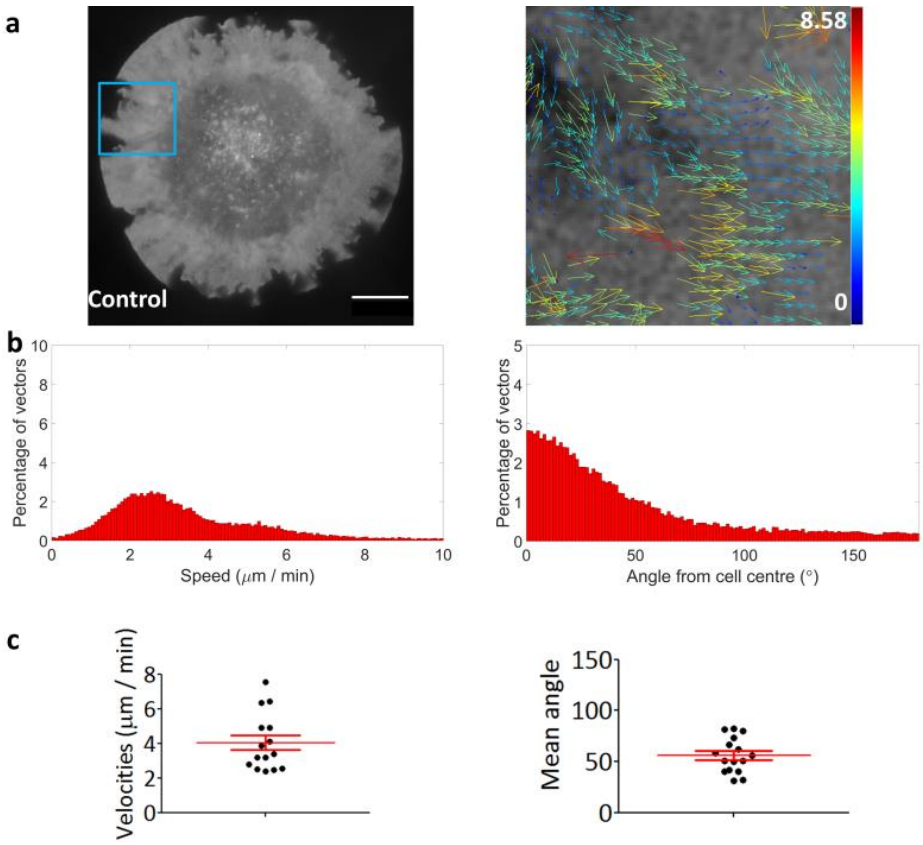

Figure 3 Characterisation of plasma membrane flow in T cells imaged with TIRF-SIM and analysed by STICS. a) The plasma membrane was labelled with the lipophilic dye DiO, and imaged 5 mins after contact with an antibody coated coverslip. Shown is a representative TIRF-SIM image with the magnified ROI within the blue box shown on the right, indicating the output vector map from STICS analysis. Scale bar = 5 µm. b) Histograms showing the velocities (left) and directionality (right) of plasma membrane flow, aggregated and normalised. c) Scatterplots of cell averages showing speeds (left: 4.00 ± 1.61 µm) and directionality (right) (n = 16).

To ensure the detected flow within the membrane was not a SIM-artefact, homogeneously distributed plate-bound fluorophores were imaged and analysed, showing reduced vector numbers (i.e. reduced detected flow) and similar random characteristics to the cell centre regions (Supplementary Figure 8). Together, these results demonstrate STICS does not correlate any artefactual features of TIRF-SIM, with fewer vectors generated from samples with static or diffusive signal.

Interference reflection microscopy (IRM) indicates that this flow may be in the form of actin ruffles which progress with a wave-like motion towards the synapse centre (Supplementary Figure 9 and Supplementary video 3). To our knowledge, this is the first demonstration of retrograde flow of the plasma membrane itself in this system. To better understand the relationship between F-actin flow and the flow of the plasma membrane, we extended the single

colour imaging method to multi-colour super-resolution microscopy in the form of two-channel TIRF-SIM and analysed the data using a cross-correlation variant STICCS[38] . Using LifeAct-GFP and the red-emitting membrane dye DiI, we were able to detect, image (Figure 4a and Supplementary video 4) and analyse actin and the membrane simultaneously.

F-actin and plasma membrane flow velocities and directionality were correlated at the immune synapse periphery indicating coupling between the two flows (Figure 4b and c). The mean ratio of the flow velocities at the periphery was 1.02 ± 0.39 (Figure 4c, left plot) indicating the flows have a similar velocity. The correlation between the directionality was also high; 0.57 ± 0.27 (where 1 indicates collinear flow) (Figure 4c, right plot) while it was observed that the correlations were reduced as the flows moved from the periphery towards the synapse centre, possibly indicating a decoupling of actin from the plasma membrane.

We next imaged cells transfected with both LifeAct-mCherry and GPI-GFP; an outer leaflet residing marker within the plasma membrane. GPI-anchored proteins have been shown to couple the inner and outer leaflets of the membrane in an actin dependent manner[39]. The correlated flow showed similar results to the LifeAct-DiI dye imaging for both velocity (1.05 ± 0.35) and directionality (0.39 ± 0.13; Supplementary Figure 10, Supplementary video 5). Importantly, these results demonstrate that the leaflets of the plasma membrane are coupled also, and the effect of the actin flow is transmitted even to extracellular leaflet components, in agreement with the active composite model. Finally, as a negative control, analysis of cytosolic-GFP did not show any significant flow and when correlated with the membrane dye DiI showed no correlated velocities (1.31 ± 0.52) or directional correlation (0.10 ± 0.13; Supplementary Figure 11).

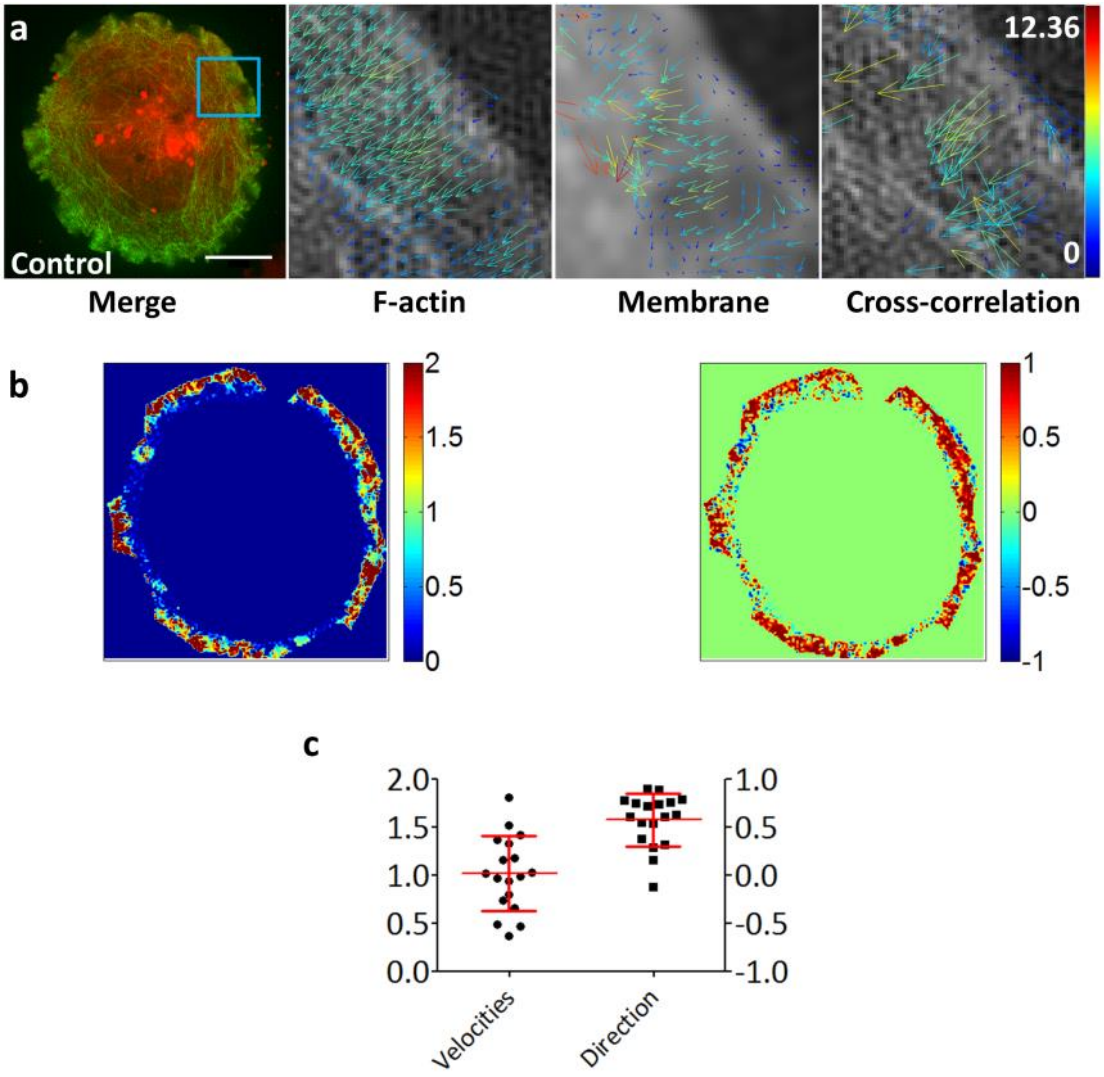

Figure 4 STICCS analysis of two-channel TIRF-SIM data. a) Jurkat T cells imaged using two-colour TIRF-SIM with F-actin labeled with EGFP-LifeAct and the plasma membrane stained with DiI. Shown are the single channel correlation outputs for actin and the plasma membrane (middle images) and the cross-correlation function between the two channels (right). Scale bar = 5 µm. b) Heatmaps show regions of greater and lesser correlation for subregion velocities (left) and directionality (right). For velocities this ratiometric measure indicates the difference between vectors where channel 1 may be flowing slower than channel 2 (giving 0), the same speed (giving +1) or flowing twice as fast (+2). Directionality is represented in a similar way, but as vector angles are established with reference to a seed point and are bound to a discrete range between 0 and 180, vectors pointing in opposite directions give -1 and those pointing in the same direction give +1. c) Scatter plots of whole cell mean velocities (left = 1.02 ± 0.39) and directionalities (right = 0.57 ± 0.27) (n = 18).

We hypothesised that the protein α-actinin, which can bind to several transmembrane proteins as well as having the ability to cross-link actin fibres[32], might act as a linker between the two. α-actinin mediates F-actin dynamics through transmembrane proteins, including those found in T cell membrane domains containing CD3[28]. Again, we used two-colour, live-cell super-resolution microscopy and quantitative cross-correlation STICCS analysis to investigate the correlation between actin flow and that of α-actinin (Figure 5 and Supplementary video 6). Our results

showed almost perfect cross-correlation between actin and α-actinin, indicating highly similar flows (Figure 5b). α-actinin was most prominent at the synapse periphery (Figure 5d) – where the correlation between the cytoskeleton flow and that of the plasma membrane was strongest.

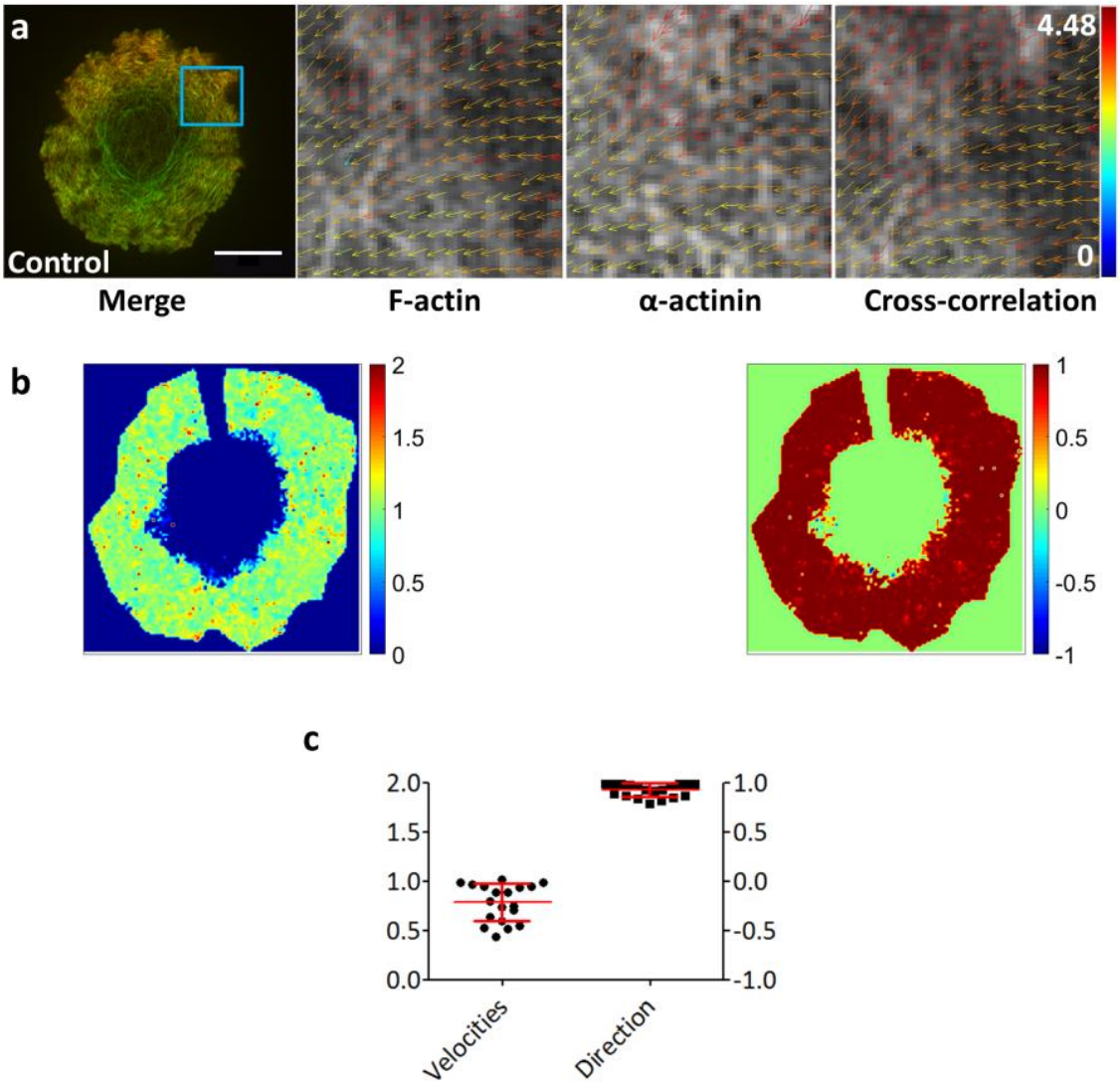

Figure 5 STICCS analysis of two-channel TIRF-SIM data. a) Jurkat T cells imaged using two-colour TIRF-SIM with F-actin labeled with EGFP-LifeAct and α-actinin labeled with mCherry (middle two images) and cross-correlation outputs (right). Scale bar = 5 µm. b) Cross correlation heatmaps of velocities (left) and directionality (right) as described in Figure 5. c) Scatter plots of whole cell mean velocities (left = 0.78 ± 0.19) and directionalities (right = 0.92 ± 0.07) (n = 19). d) Radial profile plot of single cell, showing normalised fluorescent intensity of actin and α-actinin distribution versus distance from cell centre.

Discussion:

In this study, we have applied STICS and STICCS analysis to super-resolution TIRF-SIM data, examining the flow velocities and directionality of the cortical actin cytoskeleton and the plasma membrane at the T cell immunological synapse. This extends previous studies using conventional microscopy[3,4,17], resolving dynamic details of the dense actin meshwork with quantification, at scales not previously possible. The use of super-resolution imaging is an important advance: the cortical actin mesh is extremely dense at the synapse periphery, therefore, the smaller resolution elements of SIM reduce the ensemble averaging of many independent fibres which occurs with conventional resolution microscopy. Coupling this mode of imaging with STICS allowed the quantification of flow velocities and directions over an area of the membrane which is not possible in the kymograph analysis used previously, which only computes velocities along a line profile. This is especially important for computing the angle of flow to the centre position and therefore quantifying how retrograde actin flow is.

Under control conditions, F-actin exhibited retrograde flow only at the periphery of the immune synapse. When actin polymerisation was modulated by drug treatments, this flow could be slowed and the highly orientated directionality perturbed. The plasma membrane, when imaged under control conditions, exhibited similar retrograde flow to that of F-actin and this flow was evident when observing both LifeAct-GFP and actin-GFP. Cytochalasin D, which inhibits actin polymerisation slowed actin retrograde flow, whereas Blebbistatin, which inhibits Myosin II motors had no effect. This strongly indicates the flow is driven primarily by actin polymerisation. This is the first time that such a net flow of membrane lipid components themselves has been observed.

Using two-colour super-resolution TIRF-SIM and cross-correlation analysis, it was found that the flows of the cortical actin and the plasma membrane are correlated. This analysis therefore demonstrates a potential linkage between the cortical actin meshwork and the plasma membrane. Importantly, the two leaflets of the plasma membrane were also coupled as evidenced by the correlation of GPI-GFP in the outer leaflet and actin flow. The correlation

between the two flows is apparent in super-resolved, nanoscale subregions of the membrane and is therefore not due to the micro-scale movement of the two structures. IRM data showed that the fast moving F-actin cortex at the dSMAC may drive inward flowing membrane ruffles. Such ruffling has previously been observed[40].

Correlation of the actin and membrane flow was highest in areas enriched with the actin binding protein α-actinin whose retrograde flow was highly correlated with that of actin. We therefore hypothesise that this may act as a linker between the two flowing populations. α-actinin contains actin binding domains and can also interact directly with transmembrane proteins (β-integrins) and indirectly (via Vinculin and Talin) [actinin structure paper], all of which are expressed in T cells. The cross-linking of actin directly beneath the plasma membrane may also enhance the non-specific interaction of the cytoskeleton with the membrane, thereby enhancing the "picket fence" model of cytoskeletal-membrane interactions [some kusumi shit].

This may occur within ordered phase membrane microdomains which are known to facilitate actin-membrane interactions[18] and have been observed to be enriched at the T cell synapse periphery[20].

While the role fulfilled by the cytoskeleton in regulating cell shape, organisation and polarisation is well understood[41–43], the role of the plasma membrane, beyond a platform for signal transduction, is less well known. Some reports suggest cell migration does not lead to a flowing of the membrane[44] indicating a 'slipping' of the F-actin cortex relative to the membrane, rather than creating static adhesions which can drive forces through the membrane. However,, it is known that many of the membrane and membrane-proximal proteins that are required for the regulation of T cell activation demonstrate microclustering and retrograde flow at the synapse[1,2,5,45]. We therefore hypothesise that this might also be facilitated by the retrograde flow of the plasma membrane itself which is driven by the flow of the cortical actin cytoskeleton.

Acknowledgements

The authors wish to thank Satya Khuon at the Advanced Imaging Center, Janelia Research Campus for her support, along with Deborah Keller of the FILM Imaging Centre at Imperial College London for her help with the IRM imaging. D.M.O. acknowledges European Research Council grant No. 337187 and the Marie-Curie Career Integration Grant No. 334303. P.W.W. acknowledges the Natural Sciences and Engineering Research Council of Canada's Discovery Grant program. Single-channel TIRF-SIM microscopy was carried out in the Nikon Imaging Centre, King's College London. Two-channel TIRF-SIM microscopy was performed at the Advanced Imaging Center, Janelia Research Campus, jointly sponsored by the Howard Hughes Medical Institute and the Gordon & Betty Moore Foundation. α-actinin-mCherry plasmid was a gift from the Davidson lab.

Author contributions statement

G.W.A. and D.M.O. designed the experiments. G.W.A., G.L.B. and D.J.W. carried out the cell culture, transfections, imaging and analysis. E.P. and M.H. provided STICS analysis support. R.P. carried out the IRIS imaging and reconstruction. H.E. supplied the IRIS probe. L.S. provided support for the two-channel SIM imaging. P.W.W. provided the STICS analysis code. G.W.A., G.L.B. and D.M.O. wrote the manuscript.

Competing financial interest

The authors declare no competing financial interest

References

1. Campi, G., Varma, R. & Dustin, M. L. Actin and agonist MHC-peptide complex-dependent T cell receptor microclusters as scaffolds for signaling. *J. Exp. Med.* **202,** 1031–6 (2005).

2. Beemiller, P., Jacobelli, J. & Krummel, M. F. Integration of the movement of signaling microclusters with cellular motility in immunological synapses. *Nat. Immunol.* **13,** 787–95 (2012).

3. Babich, A. *et al.* F-actin polymerization and retrograde flow drive sustained PLCγ1 signaling during T cell activation. *J. Cell Biol.* **197,** 775–87 (2012).

4. Yi, J., Wu, X. S., Crites, T. & Hammer, J. A. Actin retrograde flow and actomyosin II arc contraction drive receptor cluster dynamics at the immunological synapse in Jurkat T cells. *Mol. Biol. Cell* **23,** 834–52 (2012).

5. Varma, R., Campi, G., Yokosuka, T., Saito, T. & Dustin, M. L. T cell receptor-proximal signals are sustained in peripheral microclusters and terminated in the central supramolecular activation cluster. *Immunity* **25,** 117–27 (2006).

6. Ritter, A. T. *et al.* Actin Depletion Initiates Events Leading to Granule Secretion at the Immunological Synapse. *Immunity* **42,** 864–876 (2015).

7. Brown, A. C. N. *et al.* Remodelling of cortical actin where lytic granules dock at natural killer cell immune synapses revealed by super-resolution microscopy. *PLoS Biol.* **9,** e1001152 (2011).

8. Rak, G. D., Mace, E. M., Banerjee, P. P., Svitkina, T. & Orange, J. S. Natural killer cell lytic granule secretion occurs through a pervasive actin network at the immune synapse. *PLoS Biol.* **9,** e1001151 (2011).

9. Mace, E. M. & Orange, J. S. Lytic immune synapse function requires filamentous actin deconstruction by Coronin 1A. *Proc. Natl. Acad. Sci. U. S. A.* **111,** 6708–13 (2014).

10. Kusumi, A., Ike, H., Nakada, C., Murase, K. & Fujiwara, T. Single-molecule tracking of membrane molecules: plasma membrane compartmentalization and dynamic assembly of raft-philic signaling molecules. *Semin. Immunol.* **17,** 3–21 (2005).

11. Gowrishankar, K. *et al.* Active Remodeling of Cortical Actin Regulates Spatiotemporal Organization of Cell Surface Molecules. *Cell* **149,** 1353–1367 (2012).

12. Chichili, G. R. & Rodgers, W. Clustering of membrane raft proteins by the actin cytoskeleton. *J. Biol. Chem.* **282,** 36682–91 (2007).

13. Lillemeier, B. F., Pfeiffer, J. R., Surviladze, Z., Wilson, B. S. & Davis, M. M. Plasma membrane-associated proteins are clustered into islands attached to the cytoskeleton. *Proc. Natl. Acad. Sci. U. S. A.* **103,** 18992–7 (2006).

14. Heinemann, F., Vogel, S. K. & Schwille, P. Lateral membrane diffusion modulated by a minimal actin cortex. *Biophys. J.* **104,** 1465–75 (2013).

15. Bashour, K. T. *et al.* Cross talk between CD3 and CD28 is spatially modulated by protein lateral mobility. *Mol. Cell. Biol.* **34,** 955–64 (2014).

16. Comrie, W. A., Li, S., Boyle, S. & Burkhardt, J. K. The dendritic cell cytoskeleton promotes T cell adhesion and activation by constraining ICAM-1 mobility. *J. Cell Biol.* **208,** 457–473 (2015).

17. Yu, C., Wu, H., Kaizuka, Y., Vale, R. D. & Groves, J. T. Altered actin centripetal retrograde flow in physically restricted immunological synapses. *PLoS One* **5,** e11878 (2010).

18. Dinic, J., Ashrafzadeh, P. & Parmryd, I. Actin filaments attachment at the plasma membrane in live cells cause the formation of ordered lipid domains. *Biochim. Biophys. Acta - Biomembr.* **1828,** 1102–1111 (2013).

19. Machta, B. B., Papanikolaou, S., Sethna, J. P. & Veatch, S. L. Minimal model of plasma membrane heterogeneity requires coupling cortical actin to criticality. *Biophys. J.* **100,** 1668–77 (2011).

20. Owen, D. M. *et al.* High plasma membrane lipid order imaged at the immunological synapse periphery in live T cells. *Mol. Membr. Biol.* (2010). at <http://www.tandfonline.com/doi/full/10.3109/09687688.2010.495353>

21. Chichili, G. R., Cail, R. C. & Rodgers, W. Cytoskeletal modulation of lipid interactions regulates Lck kinase activity. *J. Biol. Chem.* **287,** 24186–94 (2012).

22. Huang, B., Bates, M. & Zhuang, X. Super-resolution fluorescence microscopy. *Annu. Rev. Biochem.* **78,** 993–1016 (2009).

23. Lillemeier, B. F. *et al.* TCR and Lat are expressed on separate protein islands on T cell membranes and concatenate during activation. *Nat. Immunol.* **11,** 90–6 (2010).

24. Williamson, D. J. *et al.* Pre-existing clusters of the adaptor Lat do not participate in early T cell signaling events. *Nat. Immunol.* **12,** 655–662 (2011).

25. Hebert, B., Costantino, S. & Wiseman, P. W. Spatiotemporal image correlation spectroscopy (STICS) theory, verification, and application to protein velocity mapping in living CHO cells. *Biophys. J.* **88,** 3601–14 (2005).

26. Ashdown, G. W., Cope, A., Wiseman, P. W. & Owen, D. M. Molecular flow quantified beyond the diffraction limit by spatiotemporal image correlation of structured illumination microscopy data. *Biophys. J.* **107,** L21–3 (2014).

27. Ashdown, G., Pandžić, E., Cope, A., Wiseman, P. & Owen, D. Cortical Actin Flow in T Cells Quantified by Spatio-temporal Image Correlation Spectroscopy of Structured Illumination Microscopy Data. *J. Vis. Exp.* e53749 (2015). doi:10.3791/53749

28. Gordón-Alonso, M. *et al.* EWI-2 association with α-actinin regulates T cell immune synapses and HIV viral infection. *J. Immunol.* **189,** 689–700 (2012).

29. Kelly, D. F. & Taylor, K. A. Identification of the beta1-integrin binding site on alpha-actinin by cryoelectron microscopy. *J. Struct. Biol.* **149,** 290–302 (2005).

30. McGregor, A., Blanchard, A. D., Rowe, A. J. & Critchley, D. R. Identification of the vinculin-binding site in the cytoskeletal protein alpha-actinin. *Biochem. J.* 225–33 (1994). at <http://www.ncbi.nlm.nih.gov/pubmed/8037676>

31. Hampton, C. M., Taylor, D. W. & Taylor, K. A. Novel structures for alpha-actinin:F-actin interactions and their implications for actin-membrane attachment and tension sensing in the cytoskeleton. *J. Mol. Biol.* **368,** 92–104 (2007).

32. Sjöblom, B., Salmazo, A. & Djinović-Carugo, K. Alpha-actinin structure and regulation. *Cell. Mol. Life Sci.* **65,** 2688–701 (2008).

33. Kiuchi, T., Higuchi, M., Takamura, A., Maruoka, M. & Watanabe, N. Multitarget super-resolution microscopy with high-density labeling by exchangeable probes. *Nat. Methods* **12,**

743–6 (2015).

34. Fiolka, R., Shao, L., Rego, E. H., Davidson, M. W. & Gustafsson, M. G. L. Time-lapse two-color 3D imaging of live cells with doubled resolution using structured illumination. *Proc. Natl. Acad. Sci. U. S. A.* **109,** 5311–5 (2012).

35. Gustafsson, M. G. L. *et al.* Three-dimensional resolution doubling in wide-field fluorescence microscopy by structured illumination. *Biophys. J.* **94,** 4957–70 (2008).

36. Thompson, R. E., Larson, D. R. & Webb, W. W. Precise nanometer localization analysis for individual fluorescent probes. *Biophys. J.* **82,** 2775–83 (2002).

37. Rentero, C. *et al.* Functional implications of plasma membrane condensation for T cell activation. *PLoS One* **3,** e2262 (2008).

38. Toplak, T. *et al.* STICCS reveals matrix-dependent adhesion slipping and gripping in migrating cells. *Biophys. J.* **103,** 1672–82 (2012).

39. Raghupathy, R. *et al.* Transbilayer lipid interactions mediate nanoclustering of lipid-anchored proteins. *Cell* **161,** 581–94 (2015).

40. Benninger, R. K. P. *et al.* Live cell linear dichroism imaging reveals extensive membrane ruffling within the docking structure of natural killer cell immune synapses. *Biophys. J.* **96,** L13–5 (2009).

41. Burkhardt, J. K., Carrizosa, E. & Shaffer, M. H. The Actin Cytoskeleton in T Cell Activation. *Annu. Rev. Immunol.* **26,** 233–259 (2008).

42. Dustin, M. L. & Cooper, J. A. The immunological synapse and the actin cytoskeleton: molecular hardware for T cell signaling. **1,** 23–29 (2000).

43. Samstag, Y. Actin cytoskeletal dynamics in T lymphocyte activation and migration. *J. Leukoc. Biol.* **73,** 30–48 (2003).

44. Kucik, D. F., Elson, E. L. & Sheetz, M. P. Cell migration does not produce membrane flow. *J. Cell Biol.* **111,** 1617–22 (1990).

45. Yokosuka, T. *et al.* Newly generated T cell receptor microclusters initiate and sustain T cell activation by recruitment of Zap70 and SLP-76. *Nat. Immunol.* **6,** 1253–62 (2005).